Calculation of Rate Constants for the $H + HI$ and $H + I_2$ Reactions Using the Semi-empirical LEPS Potential Energy Surface

Mark Cliffton C. Badlon

June 12, 2018

1 Introduction

The mechanism of the production of the production of hydrogen iodide (HI) from the mixture of H_2 and I_2 is one of the most widely discussed subjects in the field of chemical dynamics since the work of Bodenstein [1]. The history of this subject has been reviewed by Spicer and Rabinovitch citespicer. It was believed that the production of HI proceeds via a bimolecular four-center reaction between HI and I_2, for a long time. However, it was not until the 1960s that Sullivan [3] achieved a correlation of the total rate of HI formation with the rates of its elementary reactions, of which

$$H + I_2 \rightleftharpoons HI + I \tag{1}$$

$$H + HI \rightleftharpoons H_2 + I \tag{2}$$

$$H_2 + I_2 \rightleftharpoons 2\,HI \tag{3}$$

$$I_2 \rightleftharpoons 2\,I \tag{4}$$

were considered to be the dominant steps and proposed that the four-center reaction is not the main process. In the reaction mechanism presented by Sullivan, the reaction of H + HI was also included. However, the measurement on the absolute rate constant for this reaction are limited [4], although the rate constants for similar reactions such as H + HF, H + HCl, and H + HBr [5–7] have been determined by several investigators. Umemoto and co-workers [8] was the first to conduct experimental measurements by employing a pulse radiolysis-resonance absorption technique and theoretical calculations by transition state theory on the basis of an extended London-Eyring-Polanyi-Sato (LEPS) [9] surface on the H + HI system and its isotopic variants. Two decades later, an ab Initio and Density Functional Theory (DFT) study was carried

out by Canneaux and co-workers [10] to calculate the rate constants for the the gas-phase reactions of iodine atoms ($^2P_{3/2}$) with H_2, H_2O, HI, and OH. The determination of the rate constant for the H + HI reaction is also important from the practical side, because HI is one of the most widely used H atom sources.

In this present work, the semi-empirical London-Eyring-Polanyi-Sato (LEPS) potential function was used for the title reactions to carry out the following:

1. Construct a plausible potential energy surface (PES).
2. Use the PES to find the dimensions and energy of the activated complex using the Newton-Raphson optimization method.
3. Determine the classical activation energy for the system.
4. Take sections through the surface at the transition state to find the force constants, vibrational frequencies and zero-point energy of the complex.
5. Use the zero-point energies to correct the classical activation energy.
6. Calculate the Arrhenius factor (Arrhenius) from the molecular properties using statistical thermodynamics.
7. Calculate the rate constant at different temperatures.
8. Compare the calculated quantities with experimental values.

2 Theory

2.1 Transition State Theory

Transition state theory provides an approach to explain the temperature and concentration dependence of the rate law. For example, for the elementary reaction

$$H + HI \longrightarrow H_2 + I \tag{5}$$

In principle, this theory uses the potential energy surface for a triatomic system to decide the reaction coordinate, i.e., the path from reactants to products which requires passage over the lowest energy barrier.

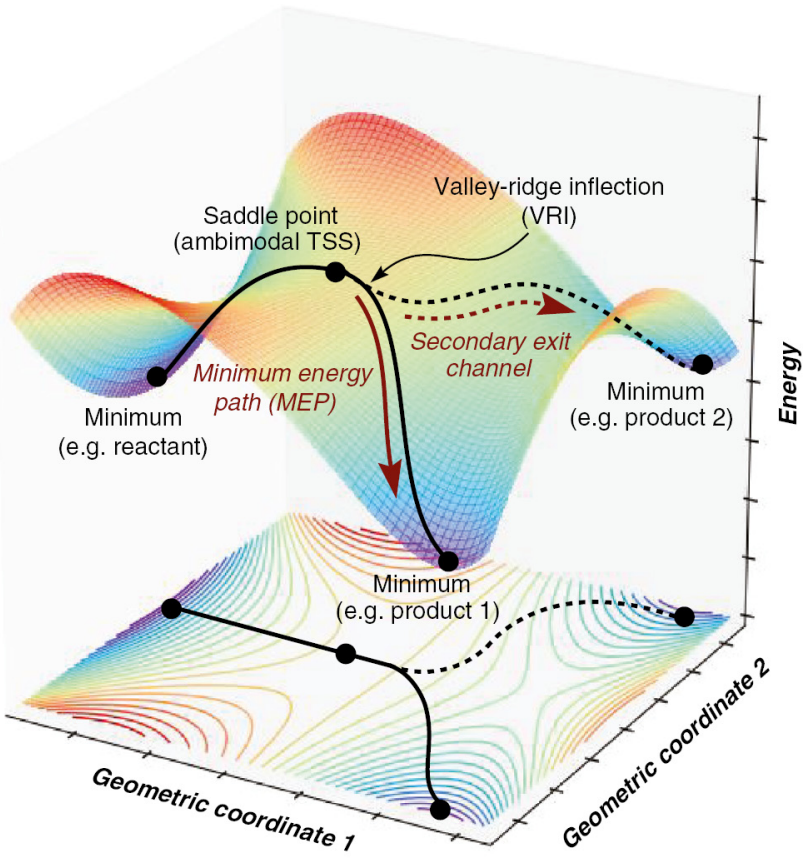

Figure 1: Potential Energy Surface

Figure 1 clearly shows reactant and product valleys separated by a low col, or saddle point. The energy of the transition state relative to the reactants determines the classical activation energy of the reaction (disregarding zero-point vibrational energies).

The rate law is

$$-r_{\mathrm{H}} = k[\mathrm{H}][\mathrm{HI}] = A\exp\left(-\frac{E_A}{RT}\right)[\mathrm{H}][\mathrm{HI}] \tag{6}$$

For simple reactions, transition state theory can predict the activation energy (E_A) and the Arrhenius factor (A) in concert with computational chemistry. In transition state theory (TST), an activated is formed during the reaction at the transition state between products from reactants.

$$\mathrm{H} + \mathrm{HI} \rightleftharpoons [\mathrm{H}{-}\mathrm{H}{-}\mathrm{I}]^{\ddagger} \longrightarrow \mathrm{H}_2 + \mathrm{I} \tag{7}$$

The rate of reaction is equal to the product of the frequency, ν_{I}, of the activated complex crossing the barrier and the concentration of the transition state complex

$$-r_{\mathrm{H}} = \nu_{\mathrm{I}}[\mathrm{HII}^{\ddagger}] \tag{8}$$

The transition state molecule ($[\mathrm{H}{-}\mathrm{H}{-}\mathrm{I}]^{\ddagger}$) and the reactants are in pseudo equilibrium at the top of the energy barrier.

$$K_c^{\ddagger} = \frac{[\mathrm{HII}^{\ddagger}]}{[\mathrm{H}][\mathrm{HI}]} \tag{9}$$

Combining gives

$$-r_{\mathrm{H}} = \nu_{\mathrm{I}} K_c^{\ddagger}[\mathrm{H}][\mathrm{HI}] \tag{10}$$

Statistical and quantum mechanics is then used to evaluate $K_c^{\ddagger}$ to arrive at the equation

$$-r_{\mathrm{H}} = \left(\frac{k_{\mathrm{B}}T}{h}\right) \frac{Q'_{\mathrm{HHI}^{\ddagger}}}{Q'_{\mathrm{H}} Q'_{\mathrm{HI}}} \exp\left(-\frac{\Delta E_0}{k_{\mathrm{B}}T}\right) \tag{11}$$

where Q' is overall the partition function per unit volume and is the product of translational, vibration, rotational, and electric partition functions, that is,

$$Q' = q'_{\mathrm{T}} q'_{\mathrm{V}} q'_{\mathrm{R}} q'_{\mathrm{E}} \tag{12}$$

The individual partition functions to be evaluated are

Translational Partition Function

$$Q_{\mathrm{trans}} = \left(\frac{2\pi m k_{\mathrm{B}}T}{h^2}\right)^{3/2} V \tag{13}$$

Vibrational Partition Function

$$Q_{\mathrm{vib}} = \prod_{i=1}^{s} \frac{1}{1 - \exp\left(-hc\bar{\nu}_i / k_{\mathrm{B}}T\right)} \tag{14}$$

where $s = 3N - 5$ for linear molecules and $s = 3N - 6$ for nonlinear molecule.

Rotational Partition Function

$$Q_{\mathrm{rot}} = \frac{8\pi^2 I k_{\mathrm{B}}T}{\sigma h^2} \qquad \text{linear polyatomic molecule} \tag{15}$$

Electronic Partition Function

$$Q_{\mathrm{elec}} = \sum_i g_i \exp\left(-\frac{E_i}{k_{\mathrm{B}}T}\right) \tag{16}$$

If the transition state can be accurately located on the potential energy surface, the interatomic distances may be read off at once. The shape of the surface around the transition state also determines the vibrational properties of the complex. Thus, an appropriate potential energy surface may be used for the complete calculation of a rate constant by means of transition-state theory.

2.2 Potential Energy Surface

The methods of quantum mechanics, in principle, have provided a means of calculating the potential energy, V, of a triatomic system. In general, V will depend on three variables, i.e., three interatomic distances or two distances and an angle, as shown in Figure 2b. It is, however, a common practice to restrict the three atoms to a straight line as in Figure 2a, so that only two independent variables are required and a three-dimensional plot of the surface may then be made (Figure 1).

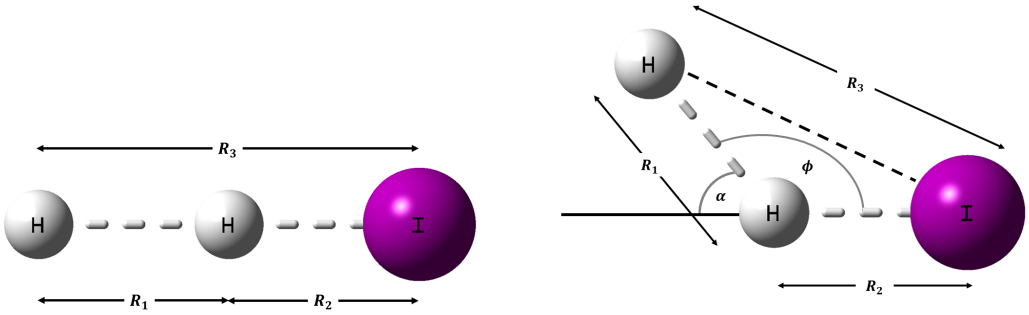

1

(a) (b)

Figure 2: Linear (a) and bent (b) configurations for a triatomic system.

Ab initio methods in quantum mechanics can provide accurate calculation of potential energies for diatomic and even polyatomic systems of molecules. However, it is also important to resort to approximate methods which could give a reasonably meaningful result. The simplest of the approximations is the Heitler-London treatment which gives the following expressions for the attractive and repulsive curves for a diatomic molecule:

$$V_{\text{att}} = \frac{Q + J}{1 + S^2} \tag{17}$$

$$V_{\text{rep}} = \frac{Q - J}{1 - S^2} \tag{18}$$

where Q is the coulombic energy arising from electrostatic attraction between electrons and nuclei, J is the exchange energy and has no classical analogy, S is the overlap integral. Q, J, and S all depend strongly on the internuclear separation. Figure 3 shows the form of the attractive and repulsive curves for H_2 and HI.

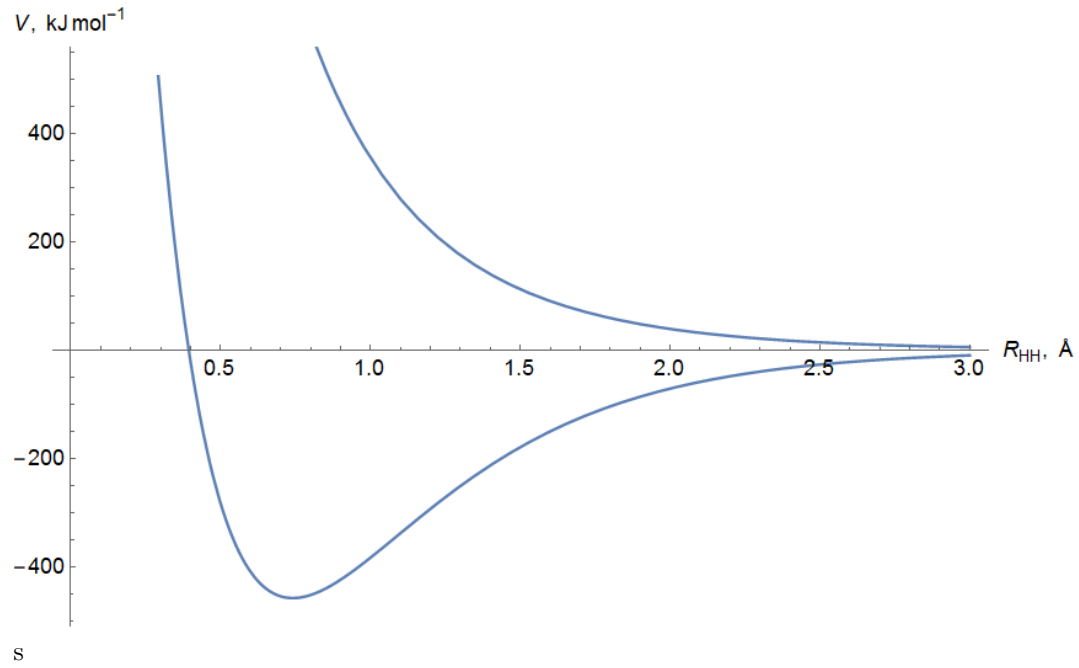

(a)

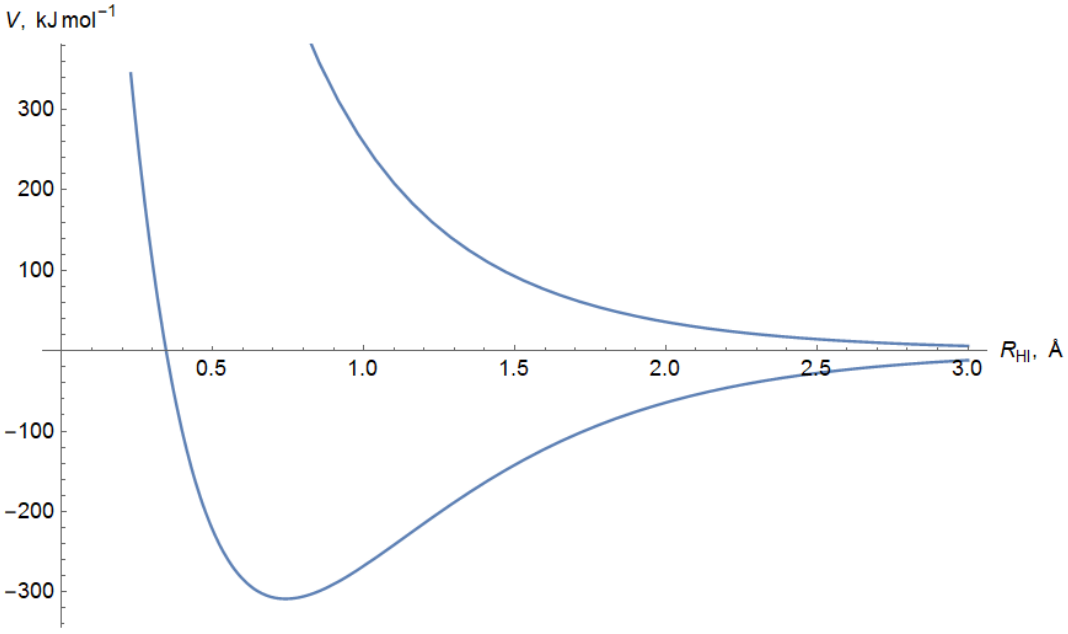

(b)

Figure 3: Morse and anti-Morse curves for (a) H_2 and (b) HI. Morse parameters are listed in Table 1.

The variation with interatomic distances of the potential energy, V, of a collinear three atom system ABC can be readily calculated by the London equation [11],

$$V_{\mathrm{L}} = Q_{\mathrm{AB}} + Q_{\mathrm{BC}} + Q_{\mathrm{AC}} \pm \left\{ \frac{1}{2} \left[(J_{\mathrm{AB}} - J_{\mathrm{BC}})^2 + (J_{\mathrm{BC}} - J_{\mathrm{AC}})^2 + (J_{\mathrm{AC}} - J_{\mathrm{AB}})^2 \right] \right\}^{1/2} \tag{19}$$

where Q_{AB}, Q_{BC}, and Q_{AC} are the coulombic interactions of the pair of electrons on the atoms of A and B,

B and C, and C and A, respectively, and J_{AB}, J_{BC}, and J_{AC} are the corresponding exchange energies. The binding energy E_A of a diatomic molecule AB is dependent on the distance R between atoms, with reference to the energy of the separated atoms as zero [12]; it is

$$V_{\mathrm{M}} = D_e \left\{ \exp\left[-2\beta(R - R_e)\right] - 2\exp\left[-\beta(R - R_e)\right] \right\} \tag{20}$$

where D_e is the classical dissociation energy (i.e., to the minimum energy curve), R_e is the equilibrium bond length and β is a constant for the molecule. Table 1 contains Morse parameters for the diatomic molecules of interest. Eyring and Polanyi [11] suggested that the coulombic energies (Q_{AB}, Q_{BC}, and Q_{AC}) are a constant fraction (q) of the total binding energies of AB, BC, and AC. The q value usually ranges from 10 to 20%. Many activation energy calculations have been carried out by using this idea know as the London-Eyring-Polanyi (LEP) method. Sato [9] modified the LEP method since the Morse equation describes only the attractive potential energy curve (empirically), Sato introduced an empirical "anti-Morse" equation to approximate the repulsive curve using the same parameters as the Morse equation. Sato's anti-Morse equation is

$$V_{\mathrm{AM}} = D_e \left\{ \exp\left[-2\beta(R - R_e)\right] + 2\exp\left[-\beta(R - R_e)\right] \right\} \tag{21}$$

Eqn. 21 was obtained from eqn. 20 by changing the sign in the bracket and dividing by two to obtain a better fit with a calculated repulsive curve for hydrogen. Figure 3 shows Morse and anti-Morse curves for H_2 and HI produced by Mathematica 11.0 [13]. Sato also offered an alternative method known as Modified London-Eyring-Polanyi-Sato (MLEPS) method where the S^2 in the Heitler-London approximation is replaced by K which is treated as an adjustable constant. The use of eqns. (18), (20), and (21) then leads to the separate expressions for Q and J in eqns. (22) and (23):

$$Q = \frac{1}{4} D_e \left\{ (3 + K)\exp\left[-2\beta(R - R_e)\right] - (2 + 6K)\exp\left[-\beta(R - R_e)\right] \right\} \tag{22}$$

$$J = \frac{1}{4} D_e \left\{ (1 + K)\exp\left[-2\beta(R - R_e)\right] - (6 + 2K)\exp\left[-\beta(R - R_e)\right] \right\} \tag{23}$$

The separate values of Q and J may then be used to calculate the potential energy for the triatomic system at any values of R_1 and R_2 by substituting in Sato's slightly modified form of the London equation

$$V_{\mathrm{Sato}} = \frac{V_{\mathrm{L}}}{1 + K} \tag{24}$$

The shape of the LEPS surface around the transition state depends strongly on the value of K. The usual way of selecting K is to choose the value which gives the best agreement with the experimental activation

energy for a particular reaction. In this study, a value of 0.17 for the adjustable constant K was chosen following the study of Moss and Coady [14].

2.3 Optimization of Transition State Geometry

The transition state properties of a particular reaction are very crucial to calculation of rate constants. The geometry of the activated complex was determined to be able to evaluate $R^{\ddagger}_{\mathrm{HH}}$, $R^{\ddagger}_{\mathrm{HI}}$, and $V^{\ddagger}$ which correspond to the bond lengths and energy of the activated complex. These parameters are required for subsequent vibrational analysis. The location of the transition state along the potential energy surface can be located using several methods. One particular example is the use of numerical optimization methods to calculate the saddle point along the potential energy surface. The Newton-Raphson method may be utilized in optimizing the initial guess to a saddle point. The principle behind the Newton-Raphson formula is the gradual improvement of an initial guess structure converging to a desired stationary point along the PES. The formula is given by

$$\mathbf{x_{n+1}} = \mathbf{x_n} - \mathbf{H^{-1}g} \tag{25}$$

where

$$\mathbf{x_{n+1}} = \begin{pmatrix} (x_{\mathrm{HH}})_{n+1} \\ (x_{\mathrm{HI}})_{n+1} \end{pmatrix} \quad = \quad \text{updated bond length matrix} \tag{26}$$

$$\mathbf{x_n} = \begin{pmatrix} (x_{\mathrm{HH}})_{n} \\ (x_{\mathrm{HI}})_{n} \end{pmatrix} \quad = \quad \text{initial bond length matrix} \tag{27}$$

$$\mathbf{H^{-1}} = \quad \text{inverse of the second derivative or Hessian matrix} \tag{28}$$

$$\mathbf{H} = \begin{pmatrix} \frac{\partial^2 V}{\partial R^2_{\mathrm{HH}}} & \frac{\partial^2 V}{\partial R_{\mathrm{HH}} \partial R_{\mathrm{HI}}} \\ \frac{\partial^2 V}{\partial R_{\mathrm{HI}} \partial R_{\mathrm{HH}}} & \frac{\partial^2 V}{\partial R^2_{\mathrm{HI}}} \end{pmatrix} = \begin{pmatrix} F_{11} & F_{12} \\ F_{21} & F_{22} \end{pmatrix} = \text{hessian} \tag{29}$$

$$\mathbf{g} = \begin{pmatrix} \left(\frac{\partial V}{\partial R_{\mathrm{HH}}}\right)_{\mathrm{HI}} \\ \left(\frac{\partial V}{\partial R_{\mathrm{HI}}}\right)_{\mathrm{HH}} \end{pmatrix} \quad = \quad \text{initial bond length matrix} \tag{30}$$

$$\tag{31}$$

Analytical evaluation requires the differentiation of the potential energy function V with respect to the appropriate variables. Numerical differentiation, on the other hand, uses approximate derivatives using the following three-point midpoint formulas:

$$\frac{\partial V}{\partial R_{\mathrm{HH}}} = \frac{1}{2h}\left[V(x_{\mathrm{HH}}+h, x_{\mathrm{HI}}) - V(x_{\mathrm{HH}}-h, x_{\mathrm{HI}})\right] \tag{32}$$

$$\frac{\partial V}{\partial R_{\mathrm{HI}}} = \frac{1}{2h}\left[V(x_{\mathrm{HH}}, x_{\mathrm{HI}}+h) - V(x_{\mathrm{HH}}, x_{\mathrm{HI}}-h)\right] \tag{33}$$

$$\frac{\partial^2 V}{\partial R_{\mathrm{HH}}^2} = \frac{1}{h^2}\left[V(x_{\mathrm{HH}}+h, x_{\mathrm{HI}}) - 2V(x_{\mathrm{HH}}, x_{\mathrm{HI}}) + V(x_{\mathrm{HH}}-h, x_{\mathrm{HI}})\right] \tag{34}$$

$$\frac{\partial^2 V}{\partial R_{\mathrm{HI}}^2} = \frac{1}{h^2}\left[V(x_{\mathrm{HH}}, x_{\mathrm{HI}}+h) - 2V(x_{\mathrm{HH}}, x_{\mathrm{HI}}) + V(x_{\mathrm{HH}}, x_{\mathrm{HI}}-h)\right] \tag{35}$$

$$\begin{aligned}\frac{\partial^2 V}{\partial R_{\mathrm{HH}}\partial R_{\mathrm{HI}}} = \frac{1}{4h^2}&[V(x_{\mathrm{HH}}+h, x_{\mathrm{HI}}+h) - V(x_{\mathrm{HH}}-h, x_{\mathrm{HI}}) \\ &- V(x_{\mathrm{HH}}, x_{\mathrm{HI}}) + V(x_{\mathrm{HH}}-h, x_{\mathrm{HI}}-h)]\end{aligned} \tag{36}$$

where the recommended values of the step size, h, vary from 0.001 to 0.01. The criteria of assigning a stationary point as optimized lies upon the gradient approaching almost zero (or close to zero) and the Hessian matrix for the TS has one negative eigenvalue. In this study, the Newton-Raphson method, using both analytical and numerical derivatives, was used to optimize the geometry of the reactants, products and the transition state (TS).

2.4 Vibration of the Activated Complex

To calculate the classical activation energy of a reaction, the LEPS potential energy function was used to obtain the potential energy surface for ABC a collinear three atom system. The stretching and bending force constants were then calculated from the PES. A linear triatomic molecule has four normal modes of vibration, two stretching vibrations and a doubly degenerate bending vibration. For an activated complex, the asymmetric stretching vibration corresponds to motion through the reaction coordinate. The vibrational frequencies are going to be used in two ways:

1. to correct the classical activation energy for zero-point energies;

2. to obtain the vibrational partition functions in the Arrhenius factor calculation.

The treatment of Johnston [15] in calculating vibrational properties of an activated complex from the PES was used.

Expanding the potential energy function in a Taylor series about the transition state give

$$V - V^{\ddagger} = \frac{1}{2}\left(\frac{\partial^2 V}{\partial R_{\mathrm{HH}}^2}\right) r_{\mathrm{HH}}^2 + \frac{1}{2}\left(\frac{\partial^2 V}{\partial R_{\mathrm{HI}}^2}\right) r_{\mathrm{HI}}^2 + \left(\frac{\partial^2 V}{\partial R_{\mathrm{HH}}\partial R_{\mathrm{HI}}}\right) \tag{37}$$

where $r_{\mathrm{HH}} = R_{\mathrm{HH}} + R_{\mathrm{HH}}^{\ddagger}$ and $r_{\mathrm{HI}} = R_{\mathrm{HI}} + R_{\mathrm{HI}}^{\ddagger}$. The stretching force constants are defined by eqs. (38)

to (40) and eq. (41) defines the bending force constant in a similar way.

$$F_{11} = \left(\frac{\partial^2 V}{\partial R_{\mathrm{HH}}^2}\right) \tag{38}$$

$$F_{22} = \left(\frac{\partial^2 V}{\partial R_{\mathrm{HI}}^2}\right) \tag{39}$$

$$F_{12} = \left(\frac{\partial^2 V}{\partial R_{\mathrm{HH}} \partial R_{\mathrm{HI}}}\right) \tag{40}$$

$$F_{\phi} = \left(\frac{\partial^2 V}{\partial \phi^2}\right)_{R_{\mathrm{HH}}, R_{\mathrm{HI}}} \tag{41}$$

The potential energy function can be well expressed in terms of three coordinates R_1, R_2 and R_3. The bending angle is related to the coordinates as

$$R_3^2 = R_1^2 + R_2^2 - 2R_1 R_2 \cos\phi \tag{42}$$

The angular force constants F_ϕ is defined by

$$\begin{aligned} F_{\phi} &= \left(\frac{\partial^2 V}{\partial \phi^2}\right) = \frac{\partial}{\partial \phi}\left(\frac{\partial V}{\partial \phi}\right) = \frac{\partial}{\partial \phi}\left(\frac{\partial V}{\partial R_3} \cdot \frac{\partial R_3}{\partial \phi}\right) \\ &= \frac{\partial V}{\partial R_3}\left(\frac{\partial^2 R_3}{\partial \phi^2}\right) + \left(\frac{\partial R_3}{\partial \phi}\right)^2 \left(\frac{\partial^2 V}{\partial R_3^2}\right) \end{aligned} \tag{43}$$

$$F_{\phi} = -\frac{R_1 R_2}{R_3}\left(\frac{\partial V}{\partial R_3}\right)_{R_1, R_2} \tag{44}$$

the values of $\dfrac{\partial R_3}{\partial \phi}$ and $\dfrac{\partial^2 R_3}{\partial \phi^2}$ are obtained from eq. (42).

The vibration frequencies, ω, are related to the force constants through the following equations:

$$\omega_i = \frac{\lambda_i^{1/2}}{2\pi} \tag{45}$$

$$\lambda_{\mathrm{sym}} = \frac{1}{2}[\mathrm{B} + (\mathrm{B}^2 - 4\mathrm{C}^2)^{1/2}] \tag{46}$$

$$\lambda_{\mathrm{sym}} = \frac{1}{2}[\mathrm{B} - (\mathrm{B}^2 - 4\mathrm{C}^2)^{1/2}] \tag{47}$$

$$B = \frac{F_{11}}{M_1} + \frac{F_{22}}{M_3} + \frac{(F_{11} + F_{22} - 2F_{12})}{M_2} \tag{48}$$

$$C = (F_{12}^2 - F_{11}F_{22})\frac{M_1 + M_2 + M_3}{M_1 M_2 M_3} \tag{49}$$

$$\lambda_{\mathrm{bend}} = F_{\phi}\left\{\frac{1}{R_1^{\ddagger 2} M_1} + \frac{1}{R_2^{\ddagger 2} M_3} + \left(\frac{1}{R_1^{\ddagger}} + \frac{1}{R_2^{\ddagger}}\right)^2 \frac{1}{M_2}\right\} \tag{50}$$

Calculation of the Force Constants

Force constants F_{11} and F_{22} are easily evaluated by taking sections through the surface at the transition state parallel to the R_{HH} and R_{HI} axes. If the PES is close to parabolic, then the force constants may be calculated as

$$F_{11} = \frac{2(V_1 - V^{\ddagger})}{r_1^2} \tag{51}$$

$$F_{22} = \frac{2(V_2 - V^{\ddagger})}{r_2^2} \tag{52}$$

The potential energy V using the LEPS expression was calculated over a range of 0.05 at a step interval of 0.01 and averages the quantities calculated from eqns.

The force constant F_{12} requires a less direct approach. The curvature of sections along some other line of slope c is used; the force constant, F_c, along this line is then given by

$$F_c = \frac{(F_{11} + c^2 F_{22} + 2cF_{12})}{(1 + c^2)} \tag{53}$$

Thus, F_{12} is obtained by rearranging the equation above to give

$$F_{12} = \frac{1}{2}(2F_c - F_{11} - F_{22}) \tag{54}$$

The bending force constant was calculated following the same procedure, except that the bond lengths in the transition state are held constant and the structure is bent out of the linear shape. The structure was bent over a 10^o range with 2^o step intervals.

2.5 Rate Constant from Transition State Theory

Ignoring the tunneling effects for bimolecular reactions, the rate constant expression using statistical mechanics as given in eqns. eqs. (13) to (16) is

$$k = \sigma \left(\frac{RT}{Lh}\right) \frac{Q^{\ddagger}}{Q_{\mathrm{A}} Q_{\mathrm{BC}}} \exp\left(-\frac{E_0}{RT}\right) \tag{55}$$

where $Q^{\ddagger}$, Q_{A}, and Q_{BC} are the partition functions expressed relative to the same energy zero and is a factor determined by the number of reaction channels available. The Arrhenius factor can also be equated to the pre-exponential term in eq. (55), leading to

$$A = \sigma \left(\frac{RT}{Lh}\right) \frac{Q^{\ddagger}}{Q_{\mathrm{A}} Q_{\mathrm{BC}}} \tag{56}$$

3 Results and Discussion

For the HHI and IHH systems, potential energy surface were constructed in order to come up with a good initial guess as to the geometry of the transition. Figures 6 and **??** show the three dimensional plots of the PES for the HHI and IHH systems, respectively. From there, the minimum energy path (MEP) along the reactant and product valley is evident. Along the MEP is a saddle shaped region which represents the approximate geometry of the transition state. Similarly, contour plots (Figures 5 and 7) were constructed to aid in approximating the bond lengths of the activated complex. Based on these plots, a point on the quadratic region or the MEP was chosen as an initial guess. Using this initial guess, the Newton-Raphson optimization scheme was utilized to arrive at a stationary point corresponding to the geometry of the transition state.

Tables 1 to 4 below summarize how the initial guesses were updated using the Newton-Raphson method. Optimization using analytic and numeric gradients and Hessians converge on a different values of $R^{\ddagger}_{\mathrm{HH}}$ and $R^{\ddagger}_{\mathrm{HI}}$. However, the use of numerical derivatives was used to be consistent with the numerical force constants calculation done by Moss and Coady [14]. It is worth to note that in contrast to the work of Moss and Coady [14], they weren't able to get a barrier for the hydrogen-iodine reactions, whereas this work was able to calculate the barrier heights, Arrhenius factors, and rate constants for the title reactions. The geometry of the stationary point was then utilized to calculate for the force constants of the transition state.

Analytical calculations of the force constants were done using eqns. 38 to 41 and numerical calculations of the force constants were also done by using the method described in Section 2.4. The force constants F_{11} and F_{22} were easily evaluated numerically by taking the section through the surface at the transition state parallel to the $R^{\ddagger}_{\mathrm{HH}}$ and $R^{\ddagger}_{\mathrm{HI}}$ axes. Then the force constants were calculated using eqns. 51 and 52. Similarly, F_{12} was calculated using eq. (54). For the bending force constant F_{ϕ}, esentially the same procedure was followed, except that the bond lengths in the transition state are held constant and the structure is bent out of the linear shape. The numerical calculations are summarized in Tables 5 and 5. Numerical force constant calculations for the HHI system is not shown, since similar values were obtained for the force constants with F_{11} and F_{22} values only being interchangeable.

Once the force constants have been determined, the calculation of the vibrational frequencies is straightforward and is easily carried out using eqs. (45) to (46).

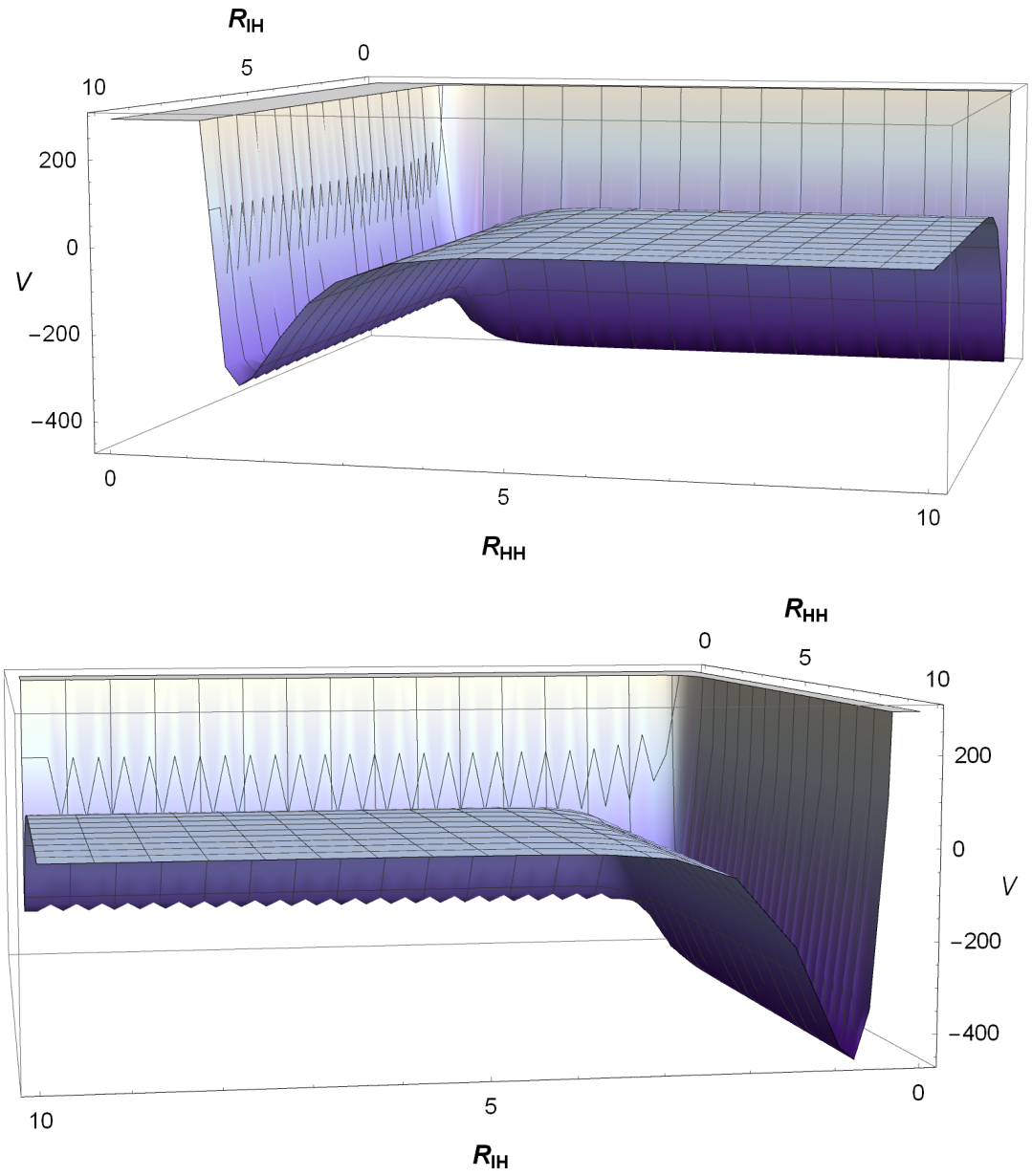

Figure 4: Potential Energy Surface for the H-H-I sytem $K = 0.17, \alpha = 0^o$.

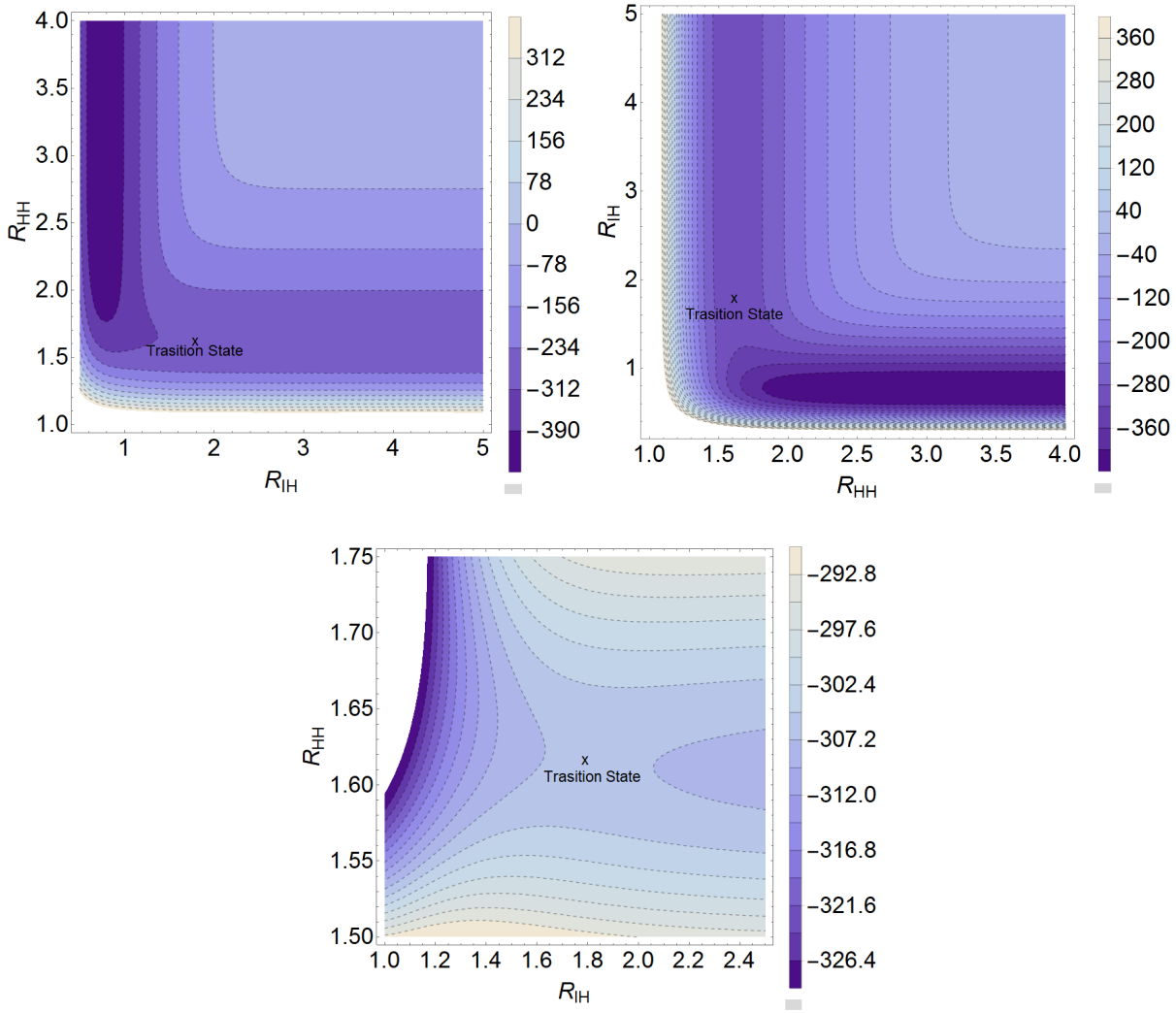

Figure 5: Contour plots for the H-H-I sytem $K = 0.17, \alpha = 0^o$.

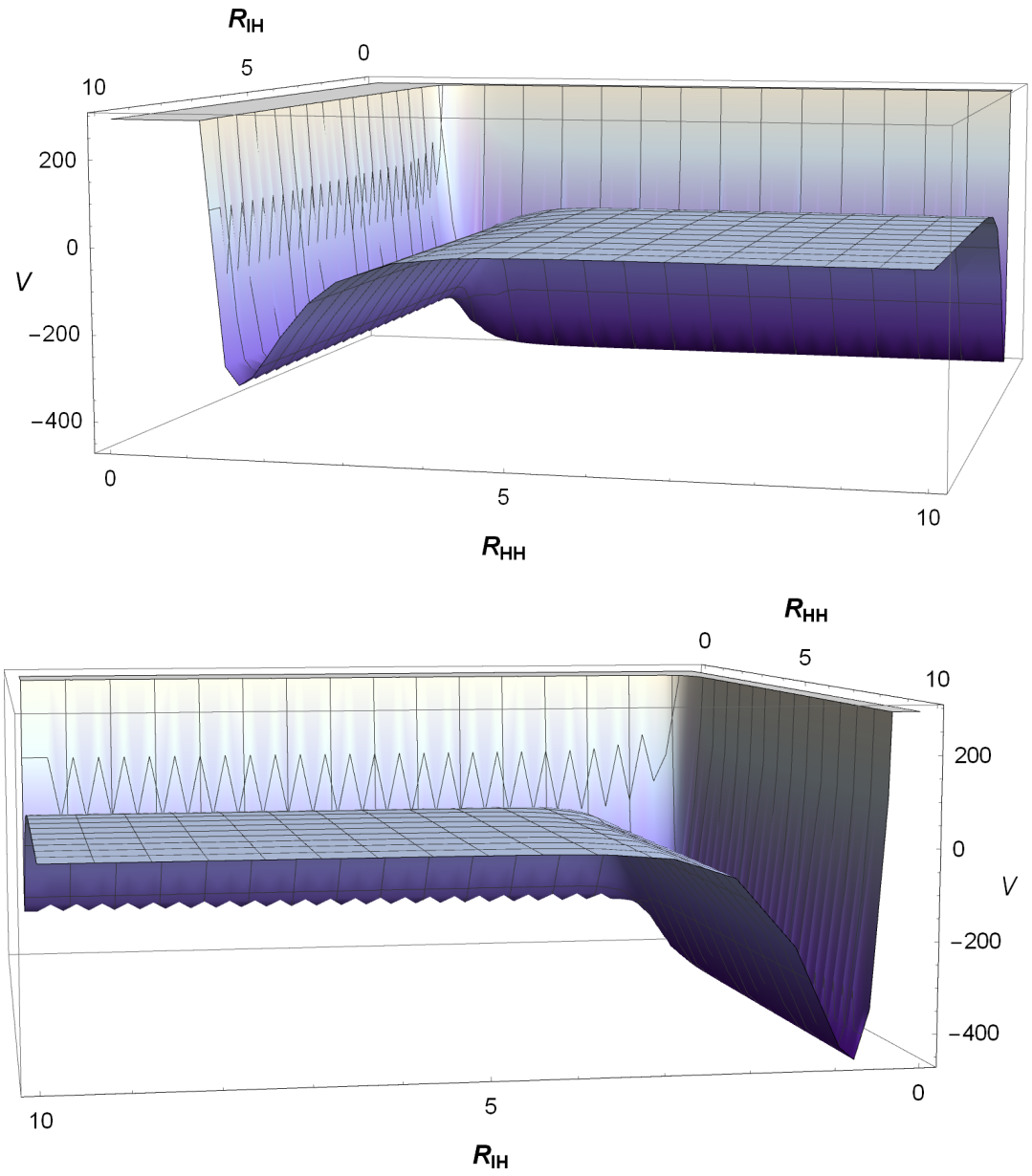

Figure 6: Potential Energy Surface for the H-H-I sytem $K = 0.17, \alpha = 0^o$.

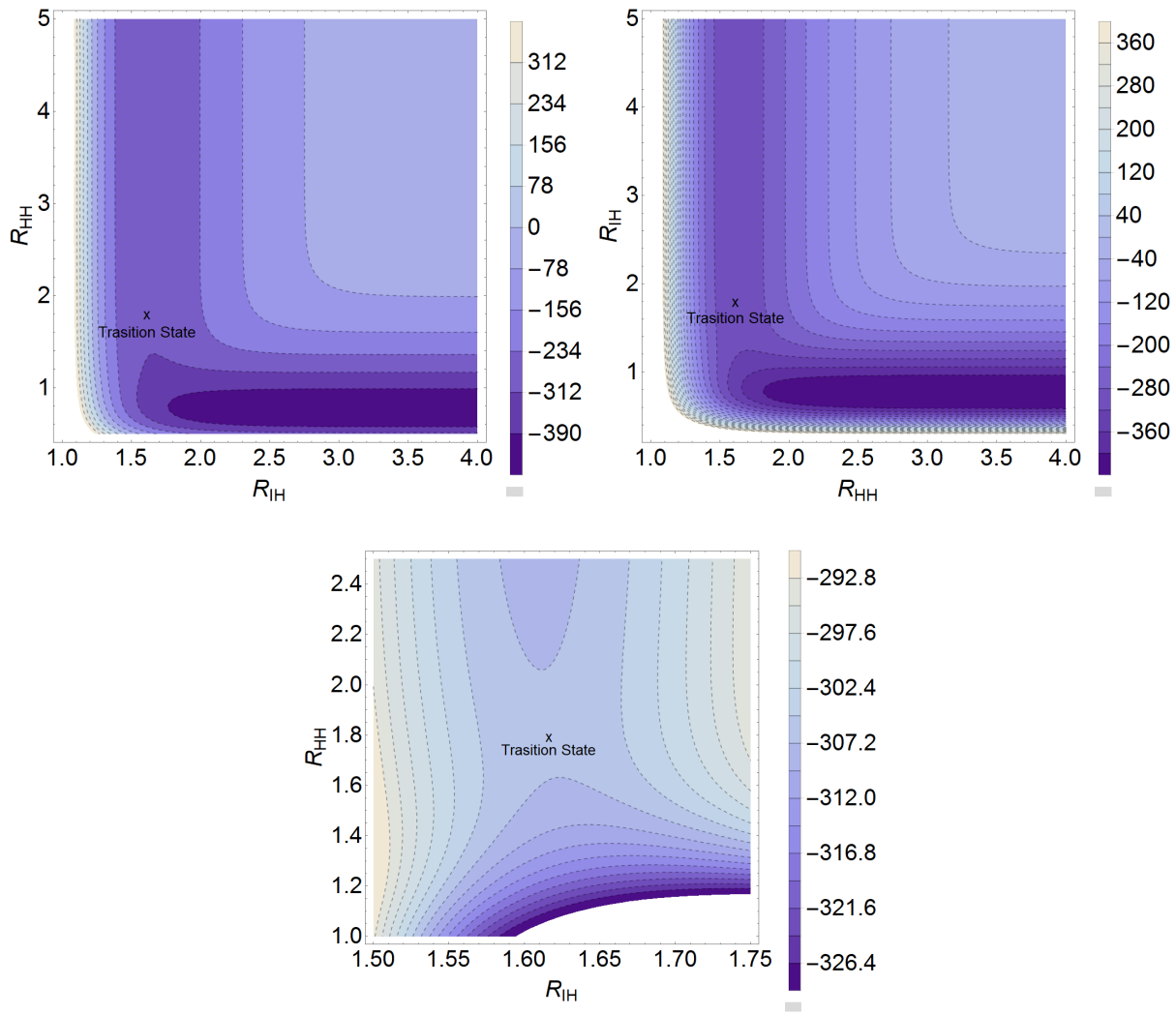

Figure 7: Contour plots for the I-H-H sytem $K = 0.17, \alpha = 0^o$.

Table 1: Saddle Point Optimization Using Numerical Derivatives ($K = 0.17, \alpha = 0^o$) for the H+HI $\longrightarrow$ H_2+I.

n	$\mathbf{x_n}$	**g**	Hessian Matrix, **H**	eigenvalues of **H**	$\mathbf{x_{n+1}}$
0	{1.50000,1.80000}	{51.92, 158.01}	{-242.79,250.38, 250.38,468.22}	{547.54,-322.11}	{1.41352,1.50877}
1	{1.41352,1.50877}	{-2.57, -300.10}	{-36.77,210.76, 210.76,3042.81}	{3057.17,-51.13}	{1.76812,1.58283}
2	{1.76812,1.58283}	{-1.56, -67.52}	{-10.18,56.36, 56.36,2146.89}	{2149.60,-11.61}	{1.78608,1.61381}
3	{1.78608,1.61381}	{-0.07, -5.10}	{-15.45,55.13, 55.13,1824.58}	{1826.23,-17.10}	{1.79113,1.61645}
4	{1.79113,1.61645}	{-0.001, -0.035}	{-15.49,54.24, 54.24,1799.27}	{1800.89,-17.11}	{1.79112,1.61647}
5	{1.79112,1.61647}	$\{8.06 \times 10^{-8}, 4.79 \times 10^{-6}\}$	{-15.49,54.25, 54.25,1799.07}	{1800.69,-17.11}	

Table 2: Saddle Point Optimization Using Analytical Derivatives ($K = 0.17, \alpha = 0^o$) for the H+HI $\longrightarrow$ H_2+I.

n	$\mathbf{x_n}$	**g**	Hessian Matrix, **H**	eigenvalues of **H**	$\mathbf{x_{n+1}}$
0	{1.50000,1.80000}	{51.90,158.09}	{-242.77,250.33, 250.33,468.06}	{547.37,-322.08}	{1.41332,1.50860}
1	{1.41332,1.5086}	{-2.60,-300.41}	{-36.67,210.80, 210.80,3044.87}	{3059.22,-51.02}	{1.76821,1.58269}
2	{1.76821,1.58269}	{-1.57,-67.64}	{-10.14,56.30, 56.30,2148.13}	{2149.60,-11.61}	{1.78536,1.61373}
3	{1.78536,1.61373}	{-0.06,-5.13}	{-15.50,55.27, 55.27,1825.02}	{1826.67,-17.16}	{1.79074,1.61637}
4	{1.79074,1.61637}	{-0.001,-0.036}	{-15.51,54.30, 54.30,1799.66}	{1801.29,-17.13}	{1.79072,1.61639}
5	{1.79072,1.61639}	$\{8.01 \times 10^{-8}, -2.07 \times 10^{-6}\}$	{-15.51,54.31, 54.308,1799.46}	{1801.09,-17.14}	

Table 3: Saddle Point Optimization Using Numerical Derivatives ($K = 0.17, \alpha = 0^o$) for the $I+H_2 \longrightarrow HI+I$.

n	$\mathbf{x_n}$	**g**	Hessian Matrix, **H**	eigenvalues of **H**	$\mathbf{x_{n+1}}$
0	$\{1.80000, 1.50000\}$	$\{158.01, 51.92\}$	$\{468.22, 250.38,$ $250.38, -242.79\}$	$\{547.54, -322.11\}$	$\{1.50877, 1.41352\}$
1	$\{1.50877, 1.41352\}$	$\{-300.10, -2.57\}$	$\{3042.81, 210.76,$ $210.76, -36.77\}$	$\{3057.17, -51.13\}$	$\{1.58283, 1.76812\}$
2	$\{1.58283, 1.76812\}$	$\{-67.52, -1.56\}$	$\{2146.89, 56.36,$ $56.36, -10.18\}$	$\{2148.37, -11.67\}$	$\{1.61381, 1.78608\}$
3	$\{1.61381, 1.78608\}$	$\{-5.10, -0.07\}$	$\{1824.58, 55.13,$ $55.13, -15.45\}$	$\{1826.23, -17.10\}$	$\{1.61645, 1.79113\}$
4	$\{1.61645, 1.79113\}$	$\{-0.035, -0.001\}$	$\{1799.27, 54.24,$ $54.24, -15.49\}$	$\{1800.89, -17.11\}$	$\{1.61647, 1.79112\}$
5	$\{1.61647, 1.79112\}$	$\{4.79 \times 10^{-6}, 8.06 \times 10^{-8}\}$	$\{1799.07, 54.25,$ $54.25, -15.49\}$	$\{1800.69, -17.11\}$	

Table 4: Saddle Point Optimization Using Analytic Derivatives ($K = 0.17, \alpha = 0^o$) for the $I+H_2 \longrightarrow HI+I$.

n	$\mathbf{x_n}$	**g**	Hessian Matrix, **H**	eigenvalues of **H**	$\mathbf{x_{n+1}}$
0	$\{1.80000, 1.50000\}$	$\{158.09, 51.90\}$	$\{468.06, 250.33,$ $250.33, -242.77\}$	$\{547.37, -322.08\}$	$\{1.5086, 1.41332\}$
1	$\{1.5086, 1.41332\}$	$\{-300.41, -2.60\}$	$\{3044.87, 210.80,$ $210.80, -36.67\}$	$\{3059.22, -51.02\}$	$\{1.58269, 1.76821\}$
2	$\{1.58269, 1.76821\}$	$\{-67.64, -1.57\}$	$\{2148.13, 56.30,$ $56.30, -10.14\}$	$\{2149.60, -11.61\}$	$\{1.61373, 1.78536\}$
3	$\{1.61373, 1.78536\}$	$\{-5.13, -0.06\}$	$\{1825.02, 55.27,$ $55.27, -15.50\}$	$\{1826.67, -17.16\}$	$\{1.61637, 1.79074\}$
4	$\{1.61637, 1.79074\}$	$\{-0.036, -0.001\}$	$\{1799.66, 54.30,$ $54.30, -15.51\}$	$\{1801.29, -17.13\}$	$\{1.61639, 1.79072\}$
5	$\{1.61639, 1.79072\}$	$\{2.07 \times 10^{-6}, 8.01 \times 10^{-8}\}$	$\{1799.46, 54.31,$ $54.31, -15.51\}$	$\{1801.09, -17.14\}$	

The numerical calculations are summarized in the following tables.

Table 5: Sections through LEPS Surface for I-H-H ($K = 0.17, \alpha = 0^o$).

R_{HH} (Å)	R_{HI} (Å)	$V - V^{\ddagger}$ (kJ mol^{-1})	$V - V^{\ddagger}/r^2$
Section EF			
1.616	1.791	0.000	
1.626	1.791	0.090	899.536
1.636	1.791	0.350	875.754
1.646	1.791	0.772	857.679
1.656	1.791	1.346	841.259
1.666	1.791	2.064	825.678
			Mean = 859.982
			F_{11} = 1719.96
Section CD			
1.616	1.791	0.000	
1.616	1.801	-0.001	-7.746
1.616	1.811	-0.003	-7.480
1.616	1.821	-0.007	-7.280
1.616	1.831	-0.011	-7.099
1.616	1.841	-0.017	-6.928
			Mean = -7.306
			F_{22} = -14.61
Section GH			
1.616	1.791	0.000	
1.626	1.801	0.095	472.687
1.636	1.811	0.368	460.617
1.646	1.821	0.812	451.377
1.656	1.831	1.417	442.964
1.666	1.841	2.174	434.973
			Mean = 452.524
			Fc = 905.047

Table 6: Transition-State Bending in I-H-H System ($K = 0.17, \alpha = 0^o$).

ϕ (deg/rad)	R_{HHI} (Å)	$V - V^{\ddagger}$ (kJ mol^{-1})	$V - V^{\ddagger}/\phi^2$
0 / 0.000	3.408	0.000	-
2 / 0.035	3.407	0.003	2.800
4 / 0.070	3.406	0.014	2.804
6 / 0.105	3.403	0.031	2.810
8 / 0.140	3.399	0.055	2.818
10 / 0.175	3.395	0.086	2.828
			Mean = 2.812
			F_{11} = 5.624

Table 8 summarizes the geometric properties and imaginary frequencies at the transition state. The calculated bond lengths are relatively different from the calculated bond lengths by Umemoto *et al.* [8] using the LEPS potential using an optimized Sato parameters. However, the calculated values for the bond lengths in this present work fall within the range of calculated bond lengths from DFT and *ab initio* calculations. The calculated bond parameters in this study are closer to the calculated values using the MPW1K/cc-pVTZ level of theory by Canneaux *et al.* [10].

Table 8: Structural Properties and Imaginary Frequencies for the Transition States.

Method*	$I_2 + H \longrightarrow HI + H$			
	$r(H_1 - H_2)$	$r(I - H_1)$	$r(I - H_1 - H_2)$	v_{asym}
Moss & Coady [14]	No barrier found			
Umemoto *et al.* [8]	1.620	1.620	180	1934i
MP2/cc-pVTZ	1.328	1.641	180	872i
MP2/6-311G(d,p)	1.286	1.663	180	1102i
MPW1K/cc-pVTZ	1.745	1.620	180	244i
MPW1K/6-311G(d,p)	1.641	1.633	180	351i
BHandHLYP/cc-pVTZ	1.889	1.616	180	111i
BHandHLYP/6-311G(d,p)	1.703	1.630	180	265i
This work	1.791	1.616	180	221i

$*$ Quantum chemical calculations were taken from Canneaux *et al.* [10]

It can be observe that there is a minute discrepancies on the calculated force constants for the numerical and analytical calculations. In this case, the numerical values for the force constants were chosen for the calculations of vibrational frequencies.

Table 9 summarizes the calculated force constants, vibrational frequencies, zero-point energies of the transition state and the reaction enthalpies. In comparison to the works of Umemoto *et al.* [8], there are disagreements between the calculated values for the vibrational frequencies. This may be due to the difference in the methods used for calculating the vibrational normal modes. This should be taken into account since the asymmetric and bending modes of the transition state which are very significant in the calculations of the zero-point vibrational frequencies, partition functions, and most especially the Arrhenius parameter. This disagreement, provides doubt on the results on both sides especially on the calculated bending mode.

Table 9: Structural Properties and Imaginary Frequencies for the Transition States.

Parameters	Numerical	Analytic	Umemoto *et al.* [8]
F_{11}	-14.6	-15.5	
F_{22}	1720.0	1799.5	
F_{12}	52.4	54.3	
F_{ϕ}	5.6		
ω_{sym}	2125	2174	2129
ω_{asym}	$221i$	$227i$	$1934i$
ω_{bend}	163		307
$Z^{\ddagger}$	14.6561		
ΔH	-137.414		-137.4

Table 10: Calculated Rate Constants at Different Temperatures and Arrhenius Factor in 10^{11} cm^3 molecule^{-1} s^{-1} and Barrier Heights at Different Levels of Theory for the Reaction $H + HI \longrightarrow I + H_2$ and a Comparison with Literature Data.

Method*	Temperature (K)				Arrhenius Factor, A	Barrier Height, E_0 (kJ mol^{-1})
	250	300	600	1000		
This work	3.2	4.4	14.5	34.0	0.12	2.45
CCSD(T)/cc-pVTZ//MP2/cc-pVTZ	0.6	0.7	2.0	4.4		
CCSD(T)/cc-pVQZ//MP2/cc-pVTZ	1.2	1.4	2.7	5.2		
CCSD(T)/6-311+G(3df,2p) //MP2/6-311G(d,p)	1.0	1.1	2.4	4.8		
CCSD(T)/6-311++G(3df,3pd) //MP2/6-311G(d,p)	2.1	2.2	3.3	5.8		
CCSD(T)/cc-pVTZ//MPW1K/cc-pVTZ	0.4	0.8	4.4	12.0		
CCSD(T)/6-311+G(3df,2p) //MPW1K/6-311G(d,p)	0.2	3.6	2.3	6.7		
CCSD(T)/cc-pVTZ //BHandHLYP/cc-pVTZ	0.9	1.6	8.0	22.0		
CCSD(T)/6-311+G(3df,2p) //BHandHLYP/6-311G(d,p)	0.2	0.4	2.8	8.3		
Vasileiadis and Benson, 1997 (ref [18], experiment)		2.1				
Umemoto *et al.*, 1988 (ref [8], experiment)	1.4	1.8			6.08	3.00
Lorenz *et al.*, 1979 (ref [4], experiment)	2.3	2.8			7.41	2.41
Baulch *et al.*, 1981 (ref [5], evaluation)			4.5	5.7	7.87	2.74

* Quantum chemical calculations were taken from Canneaux *et al.* [10]

Table 11: Calculated Rate Constants at Different Temperatures in cm^3 $molecule^{-1}$ s^{-1} and Barrier Heights at Different Levels of Theory for the Reaction $I + H_2 \longrightarrow HI + H(R_1)$ and a Comparison with Literature Data.

Method*	Temperature (K)				Barrier Height, E_0 (kJ mol^{-1})
	300	600	1000	1500	
This work	1.8×10^{-34}	5.3×10^{-22}	7.6×10^{-17}	3.8×10^{-15}	139.9
CCSD(T)/cc-pVTZ//MP2/cc-pVTZ	3.0×10^{-35}	1.0×10^{-22}	1.6×10^{-17}	8.9×10^{-15}	144.5
CCSD(T)/cc-pVTZ//MPW1K/cc-pVTZ	2.9×10^{-35}	2.2×10^{-22}	4.6×10^{-17}	2.8×10^{-14}	145.2
CCSD(T)/6-311+G(3df,2p)// MPW1K/6-311G(d,p)	8.7×10^{-35}	9.1×10^{-23}	2.2×10^{-17}	1.4×10^{-14}	147.6
CCSD(T)/6-311+G(3df,2p)// MP2/6-311G(d,p)	6.6×10^{-35}	1.5×10^{-22}	2.0×10^{-17}	1.0×10^{-14}	144.7
CCSD(T)/cc-pVTZ// BHandHLYP/cc-pVTZ	6.6×10^{-35}	4.3×10^{-22}	8.4×10^{-17}	4.9×10^{-14}	143.9
CCSD(T)/6-311+G(3df,2p)// BHandHLYP/6-311G(d,p)	1.3×10^{-35}	1.3×10^{-22}	2.9×10^{-17}	1.8×10^{-14}	146.8
Michael *et al.*, 2000 (ref [16], evaluation)	8.5×10^{-35}	2.0×10^{-22}	1.2×10^{-17}	5.1×10^{-15}	
Baulch *et al.*, 1981 (ref [5], evaluation)		1.5×10^{-22}	1.7×10^{-17}		

∗ Quantum chemical calculations were taken from Canneaux *et al.* [10]

Table 10 and 11 summarizes the calculated barrier heights, Arrhenius factor, and rate constants. It can be seen in Table 10 that the calculated rate constants deviates largely in comparison to the theoretical and experimental rate constants for the H + HI reaction found in literature [4, 5, 8, 18]. However, the calculated barrier heights fall within the range of experimental values. It is suggested that the large discrepancy is due to the calculated Arrhenius factor. The calculated Arrhenius factor deviates largely from the experimental values found in the representative literatures [4, 5, 8]. The temperature dependence of the computed rate constants over the studied temperature range (250-1000 K) exhibits an Arrhenius behavior at almost all levels of theory, as expected in light of the experimental data.

For the I + H_2 reaction, the calculated rate constants and barrier heights are summarized in Table 11. Unlike the HHI system, the calculated rate constants and barrier heights for the IHH system are in very good agreement with the experimental values.

4 Conclusion and Recommendation

In this report, theoretical calculations on the H + HI and I + H_2 reactions were carried out using the LEPS potential. The potential energy surface was constructed to visualize the reaction coordinates along the minimum energy path (MEP). Using the PES, the dimensions of and energy of the transition were located along the PES as a stationary point defined as the maximum on the MEP using the Newton-Raphson method. The calculated energy was used to calculate the classical activation energy for the title reactions. The force constants was also calculated by taking sections along the PES at the transition state and these force constants were utilized in calculating the vibrational frequencies and zero-point energies of the transition state. The classical activation energy was corrected with the zero-point energy to obtain the barrier heights of the reactions. Statistical thermodynamics provided the tools in calculating the partition functions leading to the evaluation of the translational, vibrational, rotational contribution to the partition functions of each species in the reactions. This lead the successful calculations of the Arrhenius factor from the calculated molecular properties. The calculated rate constants evaluated at different temperatures exhibited an Arrhenius behavior, consistent with existing theoretical and experimental data in literatures.

Despite the discrepancy on the calculated Arrhenius factor and rate constants for the HHI system, the complete application of transition state theory using LEPS surface lead to a remarkably close agreement between the calculated results in this work and the existing theoretical and experimental values found in literature.

In spite of the many assumptions in the LEPS procedure, potential energy functions of the LEPS type was still very useful in assessing the existing experimental values. The approximations in the LEPS potential is also still representative in calculating the rate constants of the H + HI and I + H_2 reactions.

Overall, the method presented in this study with its many assumptions was able to describe the potential energy surface of the HHI and IHH systems and calculate the structural properties and vibrational frequencies of the transition states, barrier heights, Arrhenius factor, and rate constants for the H + HI and I + H_2 reactions. However, it is recommended that evaluation of accurate vibrational normal modes be carried out for these reactions in order to obtain a reasonable values for the parameters that requires the accuracy of calculated vibrational frequencies. The Wilson GF-Matrix method [19] is recommended for the vibrational frequency calculations.

References

[1] See L. S. Kassel, Kinetics of Homogeneous Gas Reactions, Reinhold Publ. Comp., New York, 1932.

[2] Spicer, L. D.; Rabinovitch, B. S. *Ann. Rev. Phys. Chem.* **1970**, *21*, 349.

[3] Sullivan, J. H. *J. Chem. Phys.* **1967**, *46*, 73.

[4] Lorenz, K.; Wagner, H.Gg.; Zellner, R. *Ber. Bunsenges. Physik. Chem.* **1979**, *83*, 556.

[5] Baulch, D. L.; Duxbury, J.; Grant, S. J.; Montague, D. C. *J. Phys. Chem. Ref. Data*, **1981**, *10*, Suppl. 1.

[6] Husain, D.; Slater, N. K. H. *J. Chem. Soc. Faraday Trans. II*, **1980**, *76*, 276.

[7] Miller, J. C.; Gordon, R. J. *J. Chem. Phys.* **1981**, *75*, 5305.

[8] Umemoto, H.; Nakagawa, S.; Tsunashima, S.; Sato, S. *Chem. Phys.* **1988**, *124*, 259-263.

[9] (a) Sato, S. *J. Chem. Phys.*, **1955**, *23*, 592. (b) Sato, S. *J. Chem. Phys.*, **1955**, *23*, 2465.

[10] Canneaux, S.; Xerri, B.; Louis, F.; Cantrel, L. *J. Phys. Chem. A* **2010**,*114*, 9270-9288.

[11] Glasstone, S.; Laidler, K. J.; Eyring, H. *The Theory of Rate Processes: The Kinetics of Chemical Reactions, Viscosity, Diffusion and Electrochemical Phenomena;* McGraw-Hill: New York, 1941.

[12] Morse, P. M. *Phys. Rev.* **1929**, *34*, 57.

[13] Wolfram Research, Inc., Mathematica, Version 11.3, Champaign, IL (2018).

[14] Moss, S. J.; Coady, C. J. *J. Chem. Educ.* **1983**, *60*, 455.

[15] Johnston, H. S. *Gas Phase Reaction Rate Theory;* Ronald Press: New York, 1966.

[16] Michael, J. V.; Kumaran, S. S.; Su, M. C.; Lim, K. P. *Chem. Phys. Lett.* **2000**, *319*, 99106.

[17] Baulch, D. L.; Duxbury, J.; Grant, S. J.; Montague, D. C. Evaluated kinetic data for high-temperature reactions. Volume 4. Homogeneous gas phase reactions of halogen- and cyanide- containing species. *J. Phys. Chem. Ref. Data* **1981**, *10*, Suppl. 1.

[18] Vasileiadis, S.; Benson, S. W. *Int. J. Chem. Kinet.* **1997**, *29*, 915925.

[19] Wilson, E. B.; Decius, J. C.; Cross, P. C. *Molecular Vibrations*; Dover: New York, 1980.